Developments in the Built Environment 18 (2024) 100423

Contents lists available at ScienceDirect

Developments in the Built Environment

journal homepage: www.sciencedirect.com/journal/developments-in-the-built-environment

Non-destructive testing of reinforced concrete structures using sub-terahertz reflected waves

Chihiro Kobayashi [a], Tomoya Nishiwaki [a,*], Tadao Tanabe [b], Takahiro Oohashi [b], Hitoshi Hamasaki [b], Shuya Hikishima [b], Akio Tanaka [c], Koji Arita [c,e], Sho Fujii [d], Daisuke Sato [e], Takeshi Kidokoro [e]

[a] Tohoku University, 6-6-11-1209 Aoba Aramaki, Aoba-ku, Sendai, Miyagi, 980-8579, Japan
[b] Shibaura Institute of Technology, 3-7-5 Toyosu, Koto-ku, Tokyo, 135-8548, Japan
[c] Nippon Institute of Technology, 4-1 Gakuendai, Miyashiro-machi, Minamisaitama-gun, Saitama, 345-8501, Japan
[d] Yamagata University, 1-4-12 Kojirakawa, Yamagata, 990-8560, Japan
[e] Constec Engi,Co., 6-1-1 Heiwajima, Ota-ku, Tokyo, 143-0006, Japan

ARTICLE INFO

Keywords:
Sub-terahertz wave
Reinforced concrete structures
Camera
Non-destructive
Non-contact
Cracks
Embedded rebar

ABSTRACT

Terahertz (THz) and sub-terahertz (sub-THz) waves are unexplored waves between the infrared and microwave ranges. This range features unique characteristics of both light resolution and electromagnetic wave transmission. Sub-THz waves are part of attractive new diagnostic methods for inner objects because they are safer than normal non-destructive inspection methods involving high energy, such as X-rays. In this study, a novel non-contact and non-destructive inspection method for reinforced concrete (RC) structures using sub-THz reflection imaging is proposed to inspect the deterioration of inaccessible damaged RC structures. The results of this study confirmed that the proposed sub-THz imaging method can detect cracks and voids in concrete, as well as in metals inside or behind the concrete, based on differences in reflectance. In addition, the camera-based measurement system makes real-time on-site field measurements possible.

1. Introduction

In recent years, the deterioration of reinforced concrete (RC) structures has become an issue all over the world. Especially in Japan and other developed countries, large number of social infrastructures built during periods of rapid economic growth are aging significantly (Alexander and Beushausen, 2019). The importance of appropriate maintenance management, including investigation and diagnosis, has been highlighted. In addition, from the perspective of a decarbonized society, it is desirable to avoid demolishing buildings and extend the service life of RC structures through necessary and affordable repairs. Thus, these considerations highlight a growing need for non-contact, non-destructive inspection methods to diagnose infrastructure deterioration without compromising performance. Furthermore, if remote inspection is possible, it is expected to improve measurement efficiency and expand the applicable areas. Therefore, a new inspection method that is not only non-destructive but also non-contact is required.

Several non-destructive and micro-destructive testing methods have been proposed for RC structures. For example, for internal defects that cannot be detected by visual inspection, some of the most widely used methods include percussion inspection (Kazemi et al., 2019), ultrasonic flaw detection (Lawson et al., 2011; Choi et al., 2016) and ground penetrating radar (GPR) (Hugenschmidt and Mastrangelo, 2006; Chang et al., 2009; Laurens et al., 2005; Liu et al., 2020; Wiwatrojanagul et al., 2017). Table 1 shows a comparison between these methods. During percussion inspection, the concrete surface is knocked, which makes it possible to infer the state of internal deterioration based on the difference in the echo sound. In the case of ultrasonic waves, also a type of elastic wave, it is possible to measure the location of cracks and rebars inside concrete due to differences in acoustic impedance inside the material. Using GPR makes it possible to probe embedded rebars and voids inside concrete owing to its high penetration depth. However, these methods require contact with an object to be measured, which causes measurement problems at elevated or generally inaccessible places, thus highlighting the need for developing a method that can inspect the interior of concrete without contact.

* Corresponding author.
E-mail address: tomoya.nishiwaki.e8@tohoku.ac.jp (T. Nishiwaki).

https://doi.org/10.1016/j.dibe.2024.100423
Received 9 November 2023; Received in revised form 4 March 2024; Accepted 27 March 2024
Available online 30 March 2024
2666-1659/© 2024 Published by Elsevier Ltd. This is an open access article under the CC BY-NC-ND license (http://creativecommons.org/licenses/by-nc-nd/4.0/).

Table 1
Comparison of non-destructive inspection methods.

Method	Advantage	Disadvantage
Percussion inspection	• Simple and easy to test	• Depends on the examiner's judgment • Experience and skills required
Ground penetrating radar	• High penetration depth for deep location exploration	• Measurement at high altitude
Ultrasonic	• High penetration depth for deep location exploration	• Measurement at high altitude
Infrared thermography	• Remote Measurement • Easy to understand visually	• Limited to surface information
X-ray radiography	• High resolution and penetration depth	• Dangerous to the human body • Controlled area required
Sub-Terahertz waves	• Combining high penetration depth and resolution • Non-contact internal inspection possible	• Not sufficiently studied

Although infrared thermography and X-ray radiography are effective non-contact inspection methods, their application requires consideration of certain limitations. For example, infrared thermography can provide information on the surface layer of a building, such as spalling tiles on external walls. Because thermography measures infrared radiation emitted corresponding to the building facade temperature, it cannot obtain information on the internal conditions of concrete (Janků et al., 2017; Cheng et al., 2008; Omar and Nehdi, 2017). Conversely, X-rays can accurately detect the interior of concrete due to their high energy. However, this method has highly hazardous risk and is basically used in controlled environment such as laboratories (Michel et al., 2011; Skarzyński, 2016). On-site measurement requires establishing a controlled area and a permission for use. Therefore, it cannot be considered an easy measurement method. Several studies have focused on the non-contact exploration of concrete interiors. However, no established method exists currently (Mori et al., 2002; Sugimoto et al., 2016; Ham and Popovics, 2015; Kurahashi et al., 2018; Kotyaev et al., 2006; Shimada et al., 2019).

In addition, the decreasing number of skilled testers owing to serious labor shortages in recent years makes it imperative to determine deterioration levels more simply. For example, in percussion testing, when reverberation sound is judged by the human ear, diagnosis results may differ from person to person. Even in the case of machine recording, result judgment still requires a certain level of experience and may show a difference depending on the skill level. (Zhang et al., 2012; Sonoda et al., 2023). In the case of electromagnetic radar and ultrasonic methods, a certain level of knowledge and skill is required to analyze and discriminate measurement results (Tarussov et al., 2013; Dinh et al., 2021). Therefore, a testing method that can be visually understood immediately after measurement is required to improve inspection efficiency.

In this study, we propose a non-contact and non-destructive inspection method for RC structures using sub-terahertz (sub-THz) waves that can penetrate concrete and finishing materials, thus enabling remote diagnosis of invisible internal damage from the surface while providing information necessary for proper maintenance. Considering future practical applications, we adopted an areal measurement method using a sub-terahertz (sub-THz) camera, which has the potential to measure a wide area. We report the results of a basic study on specimens simulating cracks and reinforcing bars, as well as the results of measurements on real RC structures.

2. Measurement using Sub-THz waves

2.1. THz/Sub-THz wave

Fig. 1 shows the bandwidths of the THz and sub-THz waves. THz waves are electromagnetic waves with frequencies and wavelengths ranging between 0.3 and 10 THz and 30 μm–1 mm (in vacuum), respectively. They exhibit high permeability for non-polar materials, including concrete, but high absorptivity for polar materials, such as water. Sub-THz waves—with frequencies and wavelengths ranging between 0.03 and 0.3 THz and 1–10 mm (in vacuum), respectively—have similar properties to THz waves but exhibit higher transmission performance. The frequencies used in this study, 20–50 GHz, belong to a slightly lower region than the commonly defined Sub-THz range of 0.1–1 THz. However, our research group has been studying applications of a wide frequency range from about 0.01 to 10 THz, including even higher frequencies than this paper (Oyama et al., 2013; Kariya et al., 2013; Nakamura et al., 2014; Tanabe et al., 2010). Given this background, we have defined this range as "Sub-THz". Their wavelengths are intermediate, lying between electromagnetic radar and infrared thermography. Thus, they exhibit both transparency and directivity. They are also less energy intensive and safer for the human body than X-rays, eliminating the setup of a controlled area during the measurement (Oyama et al., 2009).

Stable generation devices for THz and sub-THz waves have only recently become feasible. Therefore, they are considered the last unexplored area in electromagnetic waves, with their utilization considered in various fields in recent years. THz time-domain spectroscopy (THz-TDS) is an analytical technique that uses THz waves (Neu and Schmuttenmaer, 2018). The dielectric constant and refractive index of the measured object can be analyzed at each frequency by emitting pulsed waves with extremely short peaks and Fourier transforming the transmitted or reflected waveforms. In addition, 3D imaging via the pulse-echo method using pulsed waves can provide information on the internal structure and chemical composition from the waveforms. This technology is effective in measuring materials with multilayered structures and is thus used to inspect historical artifacts (such as paintings and murals (Inuzuka et al., 2017; Lambert et al., 2020)), measure coatings on metallic materials (Krimi et al., 2016; Su et al., 2014; Im et al., 2017), and measure the corrosion thickness of steel materials (Xu and Jiang, 2022). Studies have also demonstrated the possibility of using continuous waves instead of pulses to detect wire breaks under the insulating covers of cables by exploiting the superior transparency of THz waves (Takahashi et al., 2014). Moreover, there are trials of THz electromagnetic waves applied to the non-destructive testing of various building materials and architectural art (Piesiewicz et al., 2007; Krügener et al., 2020).

Thus, THz and sub-THz waves have attracted attention in various fields in recent years, and their excellent transparency and resolution have been applied to non-destructive testing, where they can be inspected without compromising existing performance. As a result, these waves are considered potentially applicable to the non-destructive inspection of concrete structures because they enable non-contact internal exploration and provide visually understandable measurement results.

2.2. Previous studies on cement materials

THz waves are considered for applications in the construction field because of their high permeability to concrete and other construction materials. Measurement methods using THz waves can be broadly classified into those that use transmitted waves and those that use reflected waves.

First, an example of a measurement using transmission waves is described, as shown in item (a) of Table 2 (Nishiwaki et al., 2023). Some studies have successfully detected voids and embedded metal pieces in concrete based on a decrease in transmittance, demonstrating the

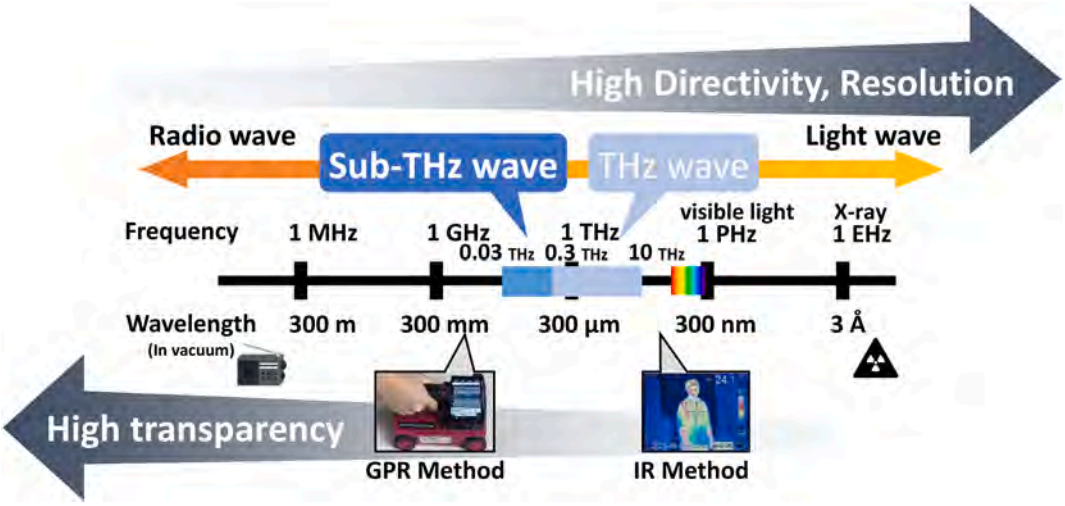

Fig. 1. Frequency bands of THz and Sub-THz waves.

Table 2
Comparison of measurement systems using Sub-THz waves.

	Conceptual Diagram	Photograph of measurement system	Characteristics
(a) Transmission (Nishiwaki et al., 2023)	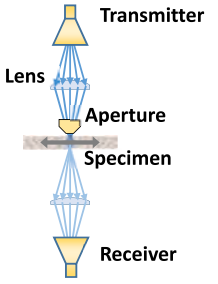	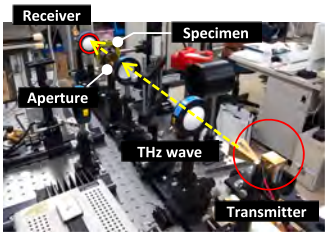	• Aperture improves resolution. • Requires equipment on both sides of the specimen. • Time-consuming measurement
(b) Reflection and half mirror (Hara et al., 2022)	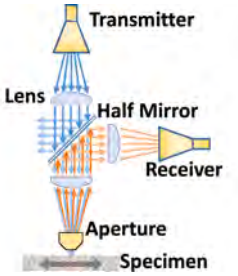	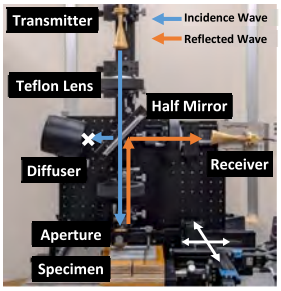	• Resolution improvement by aperture • Unsuitable for remote measurement • Time-consuming measurement
(c) Reflection and camera (Kobayashi et al., 2023)	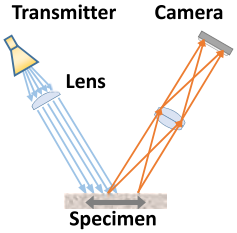	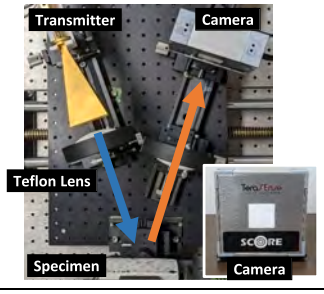	• Camera-based areal measurement • Real-time monitoring • Improved transportability due to smaller size and lighter weight

possibility of detecting internal defects in concrete using THz waves (Dash et al., 2013; Tokizane et al., 2022). In addition, THz waves easily absorbed by water have been used to detect minute cracks in concrete using water as a sensitizer and estimate the concentration of chloride ions (Oyama et al., 2009; Tripathi et al., 2012). Other studies were conducted to evaluate the self-healing effect inside self-healing concrete, which could not be confirmed visually (Nishiwaki et al., 2023).

Another measurement example using reflected waves is shown in item (b) of Table 2 (Hara et al., 2022). Studies have shown the detection of crack expansion by increasing the area of the decrease in reflectance. In addition, studies that detect invisible cracks in concrete poles have been conducted (Fan et al., 2017; Togo et al., 2012). Other studies have shown that moisture content can be estimated from reflectance using a measurement system with a half-mirror (Tanabe et al., 2018).

Although measurements using transmitted and reflected THz waves have been performed on cement materials, they have been confined to laboratory settings. As a result, issues remain to be solved for wide-area measurements of actual structures. In transmission wave measurement, it is necessary to install oscillation and detection devices on both sides of the object, which makes it difficult to move the device—particularly disadvantageous when the object is thick, for example, concrete structures. Measurements using half-mirror systems cause a large intensity attenuation when passing through the half-mirror, resulting in a lower signal-to-noise ratio. In addition, measurement systems that use an aperture to improve resolution cannot perform measurements from a distance because the aperture must be installed just in front of the test object (Tanabe and Oyama, 2019). Furthermore, in previous studies, considering only one detector element was used, images were generated by determining the reflectance in a small area at a time and were arranged in a mesh-like pattern. Although this method has the advantage of high resolution, generating images is time-consuming and does not allow for wide area scanning or real-time monitoring. Therefore, for practical applications, the measurement system must be small, lightweight, portable, and suitable for areal measurements and real-time monitoring.

As mentioned previously, existing measurement methods using sub-THz waves have problems with non-contact, wide-view monitoring of real structures. To solve this problem, we propose a novel measurement system using a sub-THz camera, as shown in item (c) of Table 2 (Kobayashi et al., 2023). The sub-THz camera has a 2.4 cm square sensor with 256 elements suitable for the sub-THz band, offering the advantages of measuring and monitoring an area in real time, as shown in Fig. 2. A GUNN diode capable of oscillating from 18 to 52 GHz was used as the source of the sub-THz wave.

Generally, the measurement error is significantly related to wavelength in optical measurements using electromagnetic waves. The frequency between 20 GHz and 50 GHz used in this study is equivalent to approximately 6 mm–15 mm wavelength in a vacuum, and approximately 2 mm–6 mm wavelength in concrete, assuming its relative permittivity of 6–8. Therefore, sub-THz measurement has the potential to detect features of at least 2 mm or more.

Before the main measurement, a test measurement was performed on a specimen with metal attached to the concrete surface, which showed a red color with greater reflection than the concrete at the metal location, confirming that real-time monitoring is possible.

3. Outline of experiment

In this study, three experimental steps were conducted using a camera-based sub-THz wave measurement system. The first step was a preliminary test using a small specimen to confirm the feasibility of the camera-based sub-THz measurement system. The second step involved a scanning test of the beam-shaped specimen. The third step was a field test wherein the developed system was used in the field and measured on an actual RC structure. In the preliminary tests, experiments were conducted on small specimens using aluminum tape and a slit. Aluminum tape was attached to the back of the specimen to simulate an embedded rebar. A slit is introduced to simulate a crack. In this scanning test, the specimens were enlarged to confirm the performance of a wide range of measurements and the actual visibility of the rebar. In a field test, the developed measurement system was used to confirm its transportability and adaptability for future practical use.

In addition, the camera is calibrated before each measurement. The sub-THz camera used in this measurement has an applicable frequency range from 10 GHz to 1 THz. However, it exhibits significant variations in detection sensitivity across different frequencies and specific sensor elements. Moreover, output data is only provided in relative values between 0 and 1. Calibration was performed at each frequency change, using an aluminum plate assumed to fully reflect sub-THz waves to have the maximum value of 1. Thus, the reflection intensity from the sample is evaluated relative to this value.

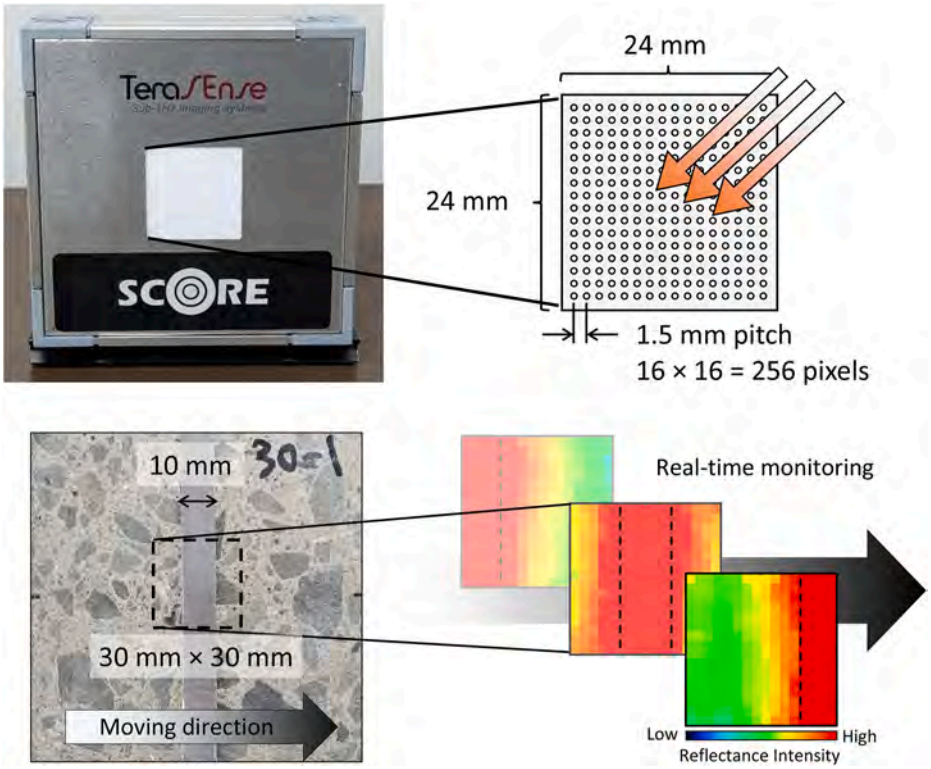

Fig. 2. Outline of the employed sub-THz camera.

4. Preliminary test with concrete plate specimens

4.1. Experimental procedures

In a preliminary test, the applicability of the measurements using sub-THz waves and a camera device was verified. An outline of the preliminary test is shown in Fig. 3. Concrete plates with widths and heights of 100 mm were prepared as specimens. Experiments were conducted on specimens with aluminum tape attached to the back-simulating rebar embedded in concrete, as shown in Fig. 3(a). In addition, specimens with slits simulating cracks with/without cover concrete (mortar) were prepared, as shown in Fig. 3(b) and (c). Table 3 summarizes the experimental parameters used in the preliminary tests. Specimens with different thicknesses were used to determine the thickness and frequency at which the metal could be detected. Measurements were also taken on pre-cut specimens with slit widths ranging between 0 and 10 mm, with the slit covered with a 5-mm-thick mortar. The measurement results were imaged as contour plots of the reflection intensity of each element.

The mix proportions used in the preliminary and subsequent scanning tests are listed in Table 4. All water–cement ratios were 0.55. Ordinary Portland cement (OPC, density 3.16 g/cm^3, specific surface area 3140 cm^2/g) was employed. Crushed sand (surface dry density 2.66 g/cm^3), and land sand (surface dry density 2.62 g/cm^3) were used as fine aggregates, while crushed stone (surface dry density 2.68 g/cm^3, maximum size 20 mm) was used as a coarse aggregate, with air-entraining admixture (AE, density 1.05 g/cm^3) also used. The slump flow of the mortar with 15 times strokes was 240 mm and the air content was 7.4%, while the slump of the concrete was 14 cm and the air content was 4.9%. The specimens were demolded one day after casting and kept in a water bath for 28 d. They were then cut to a specified thickness using a wet concrete saw. Before measurement, the specimens were dried at 60 °C for 3 d. The moisture content of the test specimens could be recognized as almost absolute dry condition. The specimens were stored in desiccators except during measurements. The measurement environment was an air-conditioned room temperature of approximately 20 °C and relative humidity of about 50%.

4.2. Backside metals measurement

Fig. 4 shows the measurement results for the concrete specimens with aluminum tape attached to the back surface. For the 10-mm-thick specimen, the reflection effect of the aluminum tape can be seen as vertical lines at the positions indicated by the dotted lines, except at 45 GHz. For the 20-mm-thick specimen, the presence of aluminum tape was confirmed at 30 and 40 GHz. However, for the 30-mm-thick specimen, a green color representing the reflective intensity of the concrete appeared at all frequencies. However, the response of the aluminum tape could not be confirmed. Additionally, concrete was represented as a uniform image, and no variations due to the presence of aggregates were observed. This is due to the negligible differences in the electrical properties between mortar and aggregates.

Table 3
Experimental parameters (preliminary test).

Category	Parameters	Variable
Backside metal	Thickness [mm]	10, 20, 30
	Aluminum tape width [mm]	10
	Frequency [GHz]	20 - 50, every 5 GHz
Slit	Thickness [mm]	10
	Slit width [mm]	0, 1, 2.5, 5, 10
	Covering material	None, mortar 5 mm
	Frequency [GHz]	20 - 50, every 5 GHz

Table 4
Mortar and concrete mix proportion.

	Unit weight (kg/m^3)				
	Water	OPC	Sand	Gravel	AE
Mortar	301	547	1368		
Concrete	168	306	790	1053	1.38

The non-response at 45 GHz and the metal position sometimes showing a stronger red color than the concrete alone or a weaker blue color than the concrete is possibly attributed to the interference between the incident and reflected waves or those reflected on the concrete surface and those reflected on the metal surface. For example, when the metal position is represented in red, the reflections on the concrete surface and the metal strengthen each other. When the metal position is represented in blue, they cancel each other out, resulting in a smaller reflection intensity than that of the concrete alone. These results indicate that the system is strongly affected by interference and that the degree of interference varies with frequency, thus making it necessary to determine a suitable frequency by finely changing it.

The edges of the tape were blurred at frequencies between 20 and 30 GHz, whereas at higher frequencies, the boundaries of the tape could be detected relatively clearly. Thus, when the aluminum tape was applied, the tape could be detected according to the difference in the reflection intensity up to a thickness of 20 mm. The higher the frequency, the clearer the tape boundary. Considering the relationship between wavelength and resolution, a wavelength of 30 GHz in vacuum is almost 10 mm, which is equivalent to the width of an aluminum tape. As the relative permittivity of concrete is around 6 to 8, the wavelength is even shorter in concrete. However, non-contact measurements pass though air, so the effect of measurement distance on resolution needs to be studied in the future.

4.3. Surface slit measurement

Fig. 5 shows the measurement results when the slit width was varied. The larger the slit width, the wider the range of low reflectance in the center, as confirmed at all frequencies. For a slit width of 1 mm, a decrease in the reflectance was observed only at 50 GHz. For a slit width of 2.5 mm, a decrease in reflectance was detected at 20, 30, 45, and 50 GHz. A slit width of 5 mm resulted in reduced reflectance at all

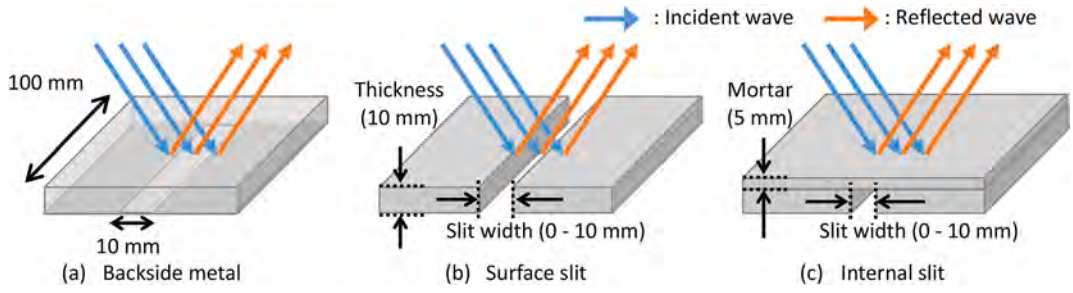

Fig. 3. Outline of preliminary test.

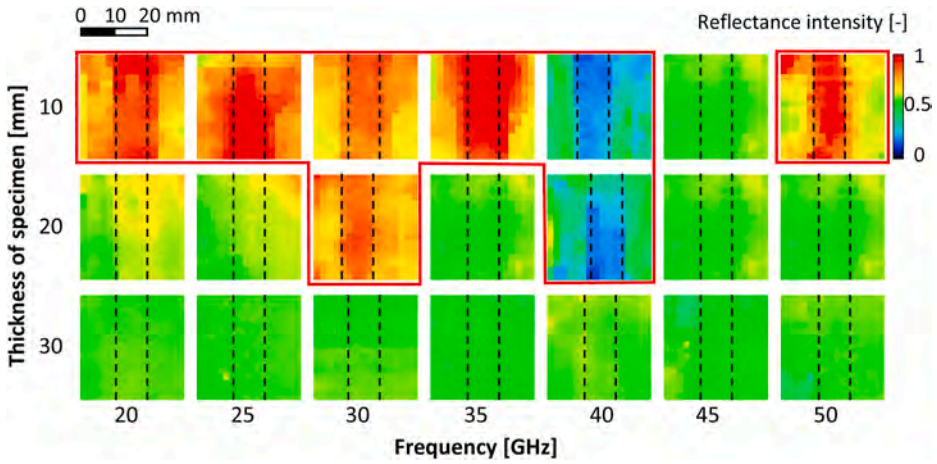

Fig. 4. Detection of aluminum tape on the back surface of concrete.

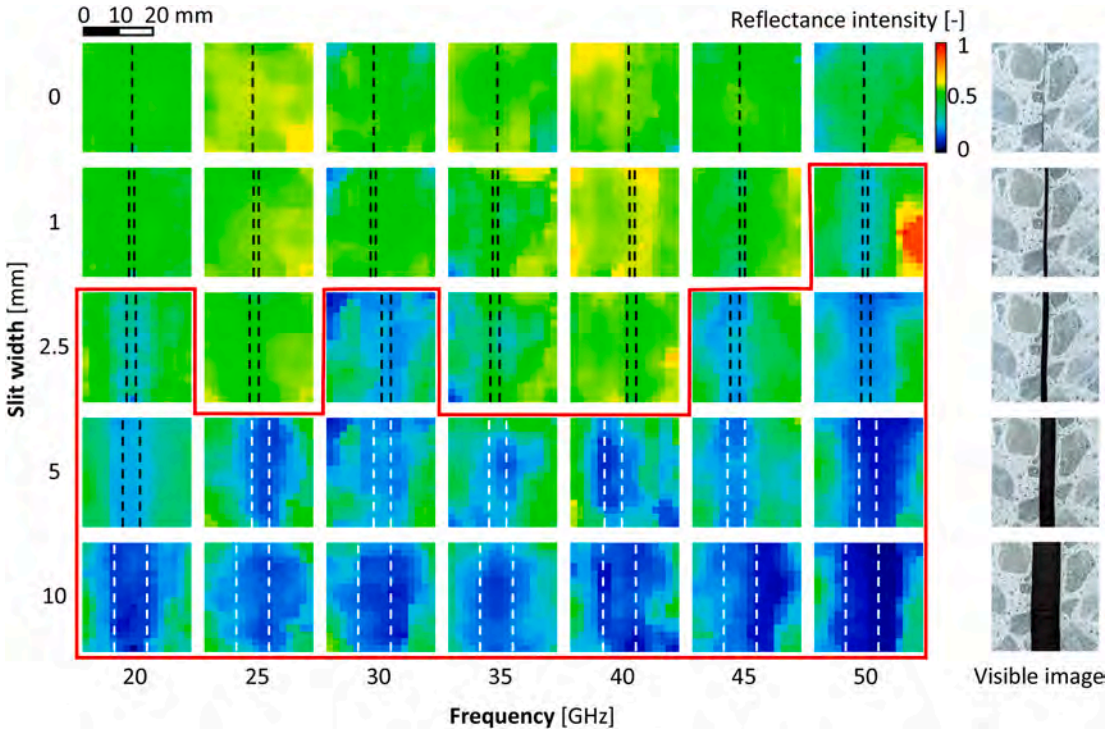

Fig. 5. Detection of surface slits.

frequencies. These results confirm that a surface slit could be detected by a decrease in reflectance. Even a slit with a narrow width of 1 mm could be detected at 50 GHz. In terms of wavelength, 50 GHz in vacuum is approximately 6 mm wavelength, which indicates that they respond to slits that are narrower than their wavelength. One possible reason is that the diagonal incidence may respond to the depth of the slit. Although relatively large slits were measured in this study, further studies are required to measure fine cracks in actual buildings.

4.4. Internal slit measurement

Fig. 6 shows the results when the slit width was varied, with the slit covered by a 5-mm-thick mortar simulating the finishing material. The slit position is blue, indicating a lower reflection intensity than the surrounding area. Although the response was generally weaker than when the slit was exposed and the detection limit of the slit width was 2.5 mm, the possibility of detecting internal voids and cracks that progressed from the inside owing to the corrosion of the steel bars was confirmed.

In this preliminary test, the measurements were carried out on a slit and metal independently. The simplified measurement targets differ from the conditions of actual structures, implying that the actual measurements would contain more complex information. The method employed here, which visualizes the measurement results at a single frequency using the camera, consolidates information into only the reflection intensity. Thus, it is still challenging to distinguish cracks, voids, metals, etc. However, the authors are currently verifying that varying frequencies can provide more detailed information. Therefore, it is anticipated that future investigations will enable to distinguish each component of aggregates, voids, metals, and so on by selecting frequencies that sensitively respond to each of the elements.

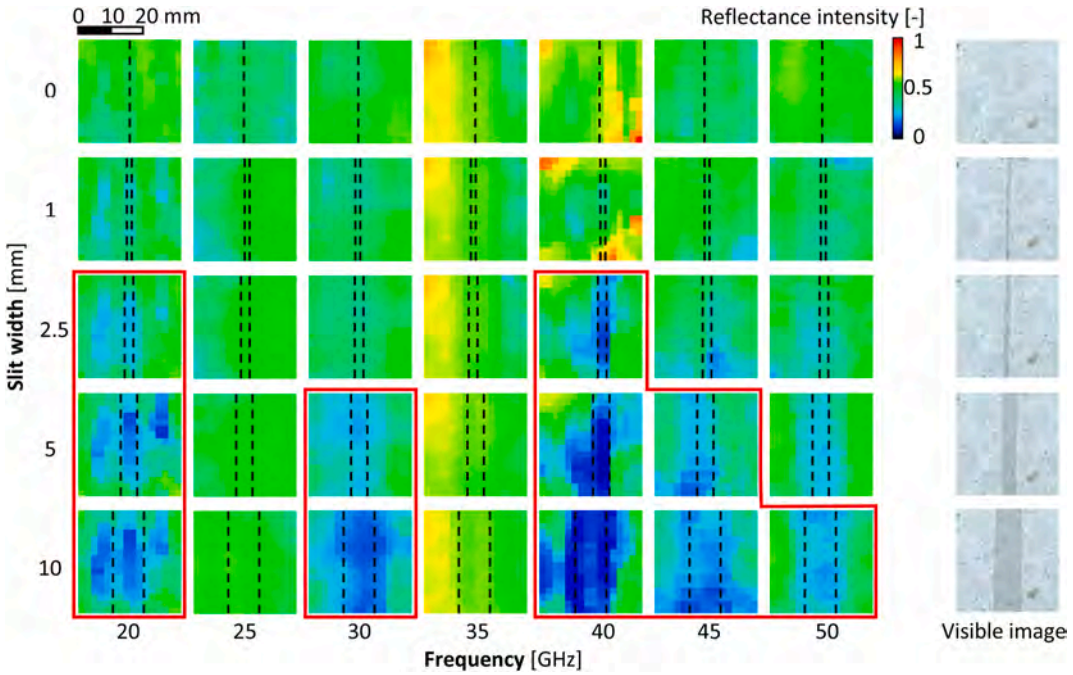

Fig. 6. Detection of internal slit.

5. Scanning test with concrete beam specimens

In the scanning test, the size of the test specimen was enlarged to a beam shape to make the measurement closer to the on-site operation, and a wide area was measured while moving the measurement system. This confirms the wide range of measurement performances for practical use. In addition, the metal measurement was changed from aluminum tape to embedded rebar to confirm the effects of shape and other factors.

5.1. Specimens and experimental parameters

An outline of the specimens used for the scanning tests is shown in Fig. 7. A beam with a width of 100 mm and length of 400 mm was used as the test specimen. Reinforcing bars with different cover thicknesses and diameters and slits of different widths were placed inside the specimen. Experimental parameters are listed in Table 5. The measurements were performed on the specimens under dry conditions. The specimens were dried at 60 °C for 3 days as in the preliminary test, therefore, the moisture content was almost absolute dry condition. The measurement environment was an air-conditioned room temperature of approximately 20 °C and relative humidity of about 50%. For the slit specimens, the slits on the surface and interior were measured using the back and front sides of the specimen. As shown in Fig. 8, the transportability and real-time monitoring performance of the field measurements were confirmed by moving a sub-THz camera device. The measurement images were created by stitching multiple images captured while moving the device.

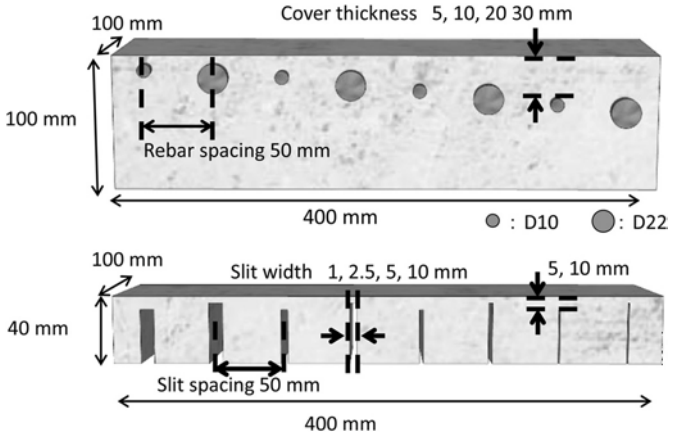

Fig. 7. Outline of the specimen (scanning measurement).

Table 5
Experimental Parameters (Scanning measurement).

Category	Parameters	Variable
Embedded rebar	Cover Thickness [mm]	5, 10, 20, 30
	Diameter [mm]	10, 22
	Frequency [GHz]	20 - 50, every 5 GHz
Slit	Thickness [mm]	10
	Slit width [mm]	1, 2.5, 5, 10
	Covering material	None, Concrete 5, 10 mm
	Frequency [GHz]	20 - 50, every 5 GHz

5.2. Measurement of embedded rebar

Fig. 9 shows images obtained at different frequencies. In the measurement of the embedded rebar, an increase in the reflection intensity can be confirmed, although there is some disturbance, presumably caused by the unevenness of the rebar. At 50 GHz, D22 and D10 are detected at a cover thickness of 5 mm, whereas D22 is detected at a cover thickness of 10 mm. An increase in the reflection intensity was also observed at deeper depths. However, the location of the rebar could not be identified. The D10 with a cover thickness of 5 mm shows a slight change in reflection intensity above 35 GHz. This indicates that shorter wavelengths than the object could be useful, as in the preliminary measurements. Regarding the penetration depth, the fact there is a slight red reaction area suggests that even at the longest wavelength of 6 mm at 50 GHz, it penetrates to a depth of about 30 mm. However, the resolution is insufficient for detecting rebar, so high radiation intensity and high frequencies need to be tested. In addition, the rebar was placed at 50 mm intervals in this study, so it is likely affected by the rebar existing next to it, and it is necessary to study a case similar to the actual rebar

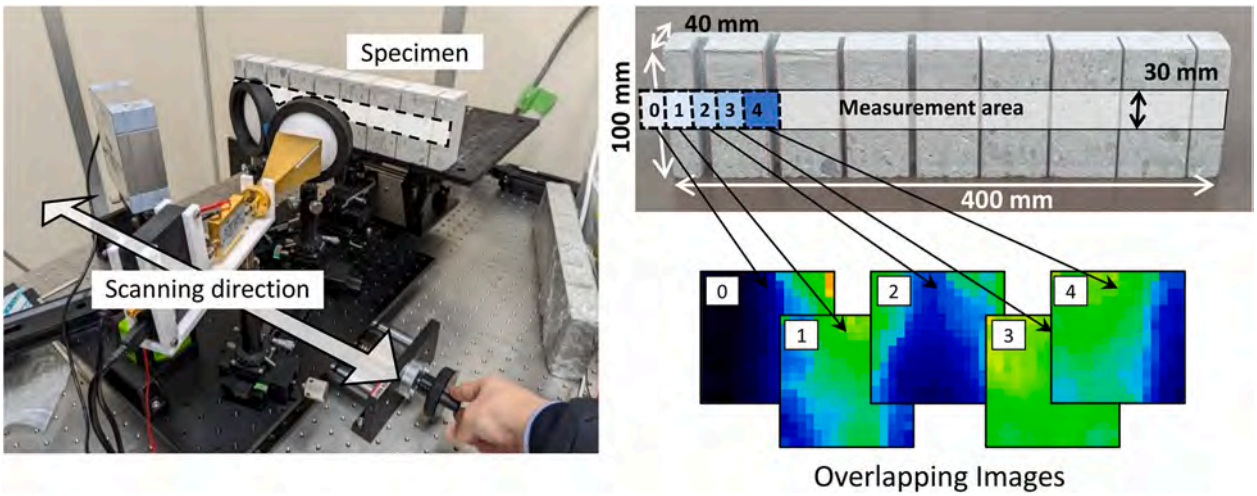

Fig. 8. Experimental procedures.

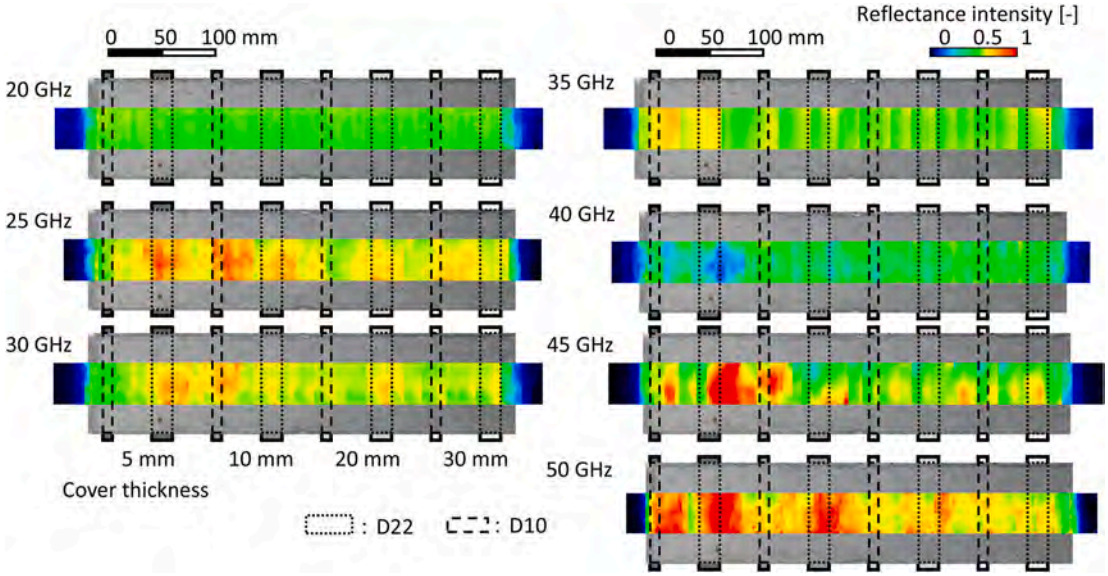

Fig. 9. Detection of embedded rebar.

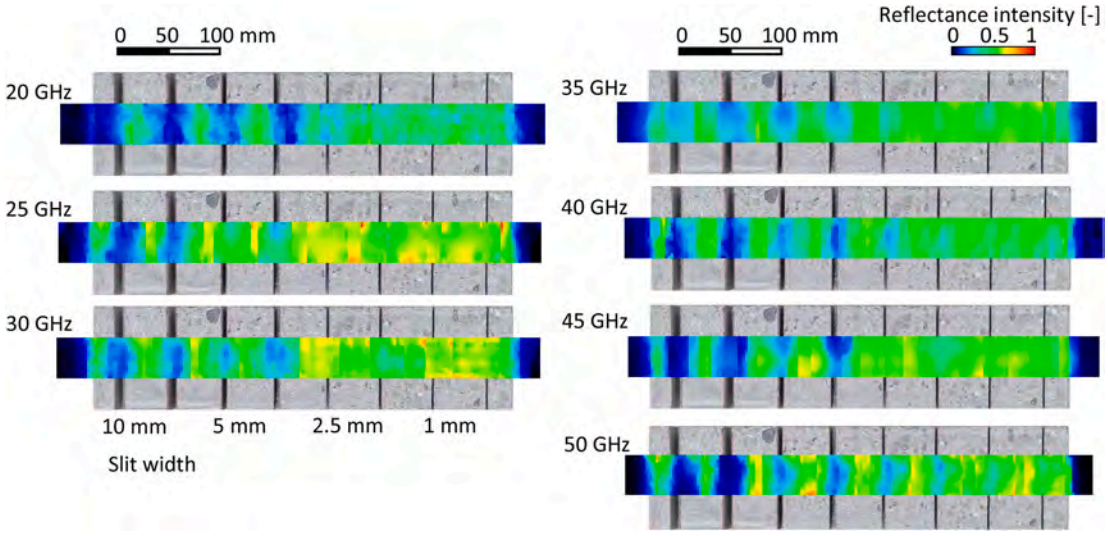

Fig. 10. Detection of surface slit.

spacing in the future.

5.3. Measurement of surface slit

Fig. 10 shows images obtained at different frequencies. From the surface slit measurement, it was confirmed that the reflection intensity decreased at the slit position, as in the preliminary test, and that the larger the slit width, the larger the affected area. The results show that slits can be clearly detected on the surface. The results suggest that slits on the surface can be detected by the penetration of sub-THz waves at the slit position and the reduction of the reflected component.

5.4. Measurement of internal slit

Fig. 11 shows images obtained at different frequencies. Even with these slits hidden inside, at low frequencies such as 20 GHz, they could be detected up to 5 mm wide and 10 mm deep because of the increase in reflection intensity, presumably owing to the increase in reflective surfaces.

The results of the internal slit measurements tended to differ from those of the preliminary measurements, with the slit position shown in blue for the preliminary measurements and the slit position being red for the scanning measurements. This phenomenon may have been caused by the difference in the layer structure created when simulating the internal slit. In the preliminary measurement, one mortar plate was placed on top of two plates arranged with a gap between them. Thus, there was a slight air gap between the concrete and mortar. In contrast, in the scanning test, the slit specimen was created by notching the beam specimen. Therefore, it was formed as a single piece without air gaps. Electromagnetic waves reflect at the boundary surfaces of different materials. In the preliminary test specimens, there is an air gap except at the slit location. Therefore, the reflection intensity is higher other than at the location of the slit due to reflections from the air gap and the concrete behind the mortal. In contrast, the boundary conditions in the scanning test were uniform, so the reflection intensity from the slit position closer to the air boundary was relatively higher.

Based on the results obtained here, further study is required to detect micro-scale cracks and voids in concrete accurately. However, this method aims to scan a wide area more efficiently rather than precisely detecting defects individually. In addition, there is a related technique called synthetic aperture processing, which is used in satellite photography and obtains high resolution even at millimeter waves. Combining this technique with the proposed method could be a promising approach to improve the accuracy with further investigation.

6. On-site measurements on Gunkanjima

6.1. About Gunkanjima

On-site measurements were conducted on Hashima Island, also known as Gunkanjima, located off the coast of Nagasaki Prefecture. Fig. 12 illustrates the current situation in Gunkanjima, Japan. Gunkanjima once prospered as a coal mining island, but with an energy shift from coal to oil, the island has closed and is now uninhabited. Owing to a lack of knowledge about deterioration at the time of construction, sea sand was used as a fine aggregate, and the inherent salt content of the concrete was extremely high. In this study, we measured the response of a structure that had deteriorated significantly due to rebar corrosion and conducted measurements on Gunkanjima Island to confirm transportability and measurement issues for practical use.

6.2. Measurement overview

The measurement object was a pillar supporting a conveyor belt used to transport coal. Fig. 13 shows the details of the measured pillar. The cross section of column was 600 mm by 600 mm and consisted of an original interior SRC structure of 400 mm by 400 mm with 100-mm-thick concrete wrapped later. Measurements of these pillars were previously conducted in Nagasaki City. Based on the results of testing cores taken from other neighboring pillars and chipping tests, the cover thickness at the measured location was approximately 35 mm, the diameter of the main rebar was 12 mm, the diameter of the ribs was 9 mm, the chloride ion content was 6.16 kg/m^3, and the compressive strength was 29 N/mm^2. The measurement ranges were approximately 30 and 500 mm in height and width, respectively. At the right end of the pillar, the cover was stripped off because of rebar corrosion, which exposed the rebar. First, the location of the main rebar was identified using GPR. Then, measurements using sub-THz waves were performed to confirm the accuracy and resolution of the measurement system, as well as the challenges of measuring in an actual structure.

6.3. Measurement results

The measurement results are shown in Fig. 14. A 10 GHz oscillator was used for the measurement. Although there are some distortions and positional gaps, an increase in the reflection intensity can be observed at

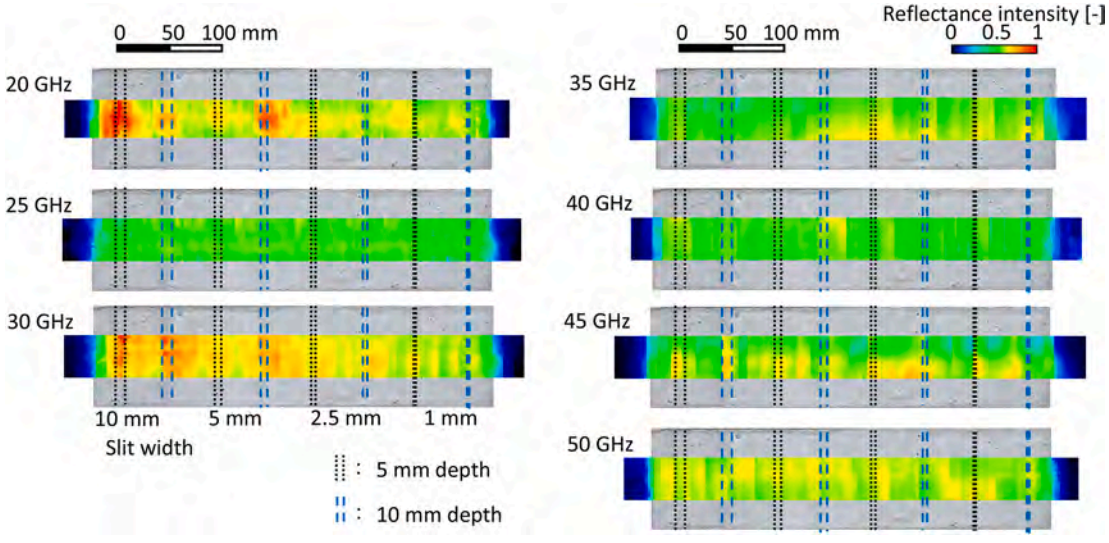

Fig. 11. Detection of internal slit.

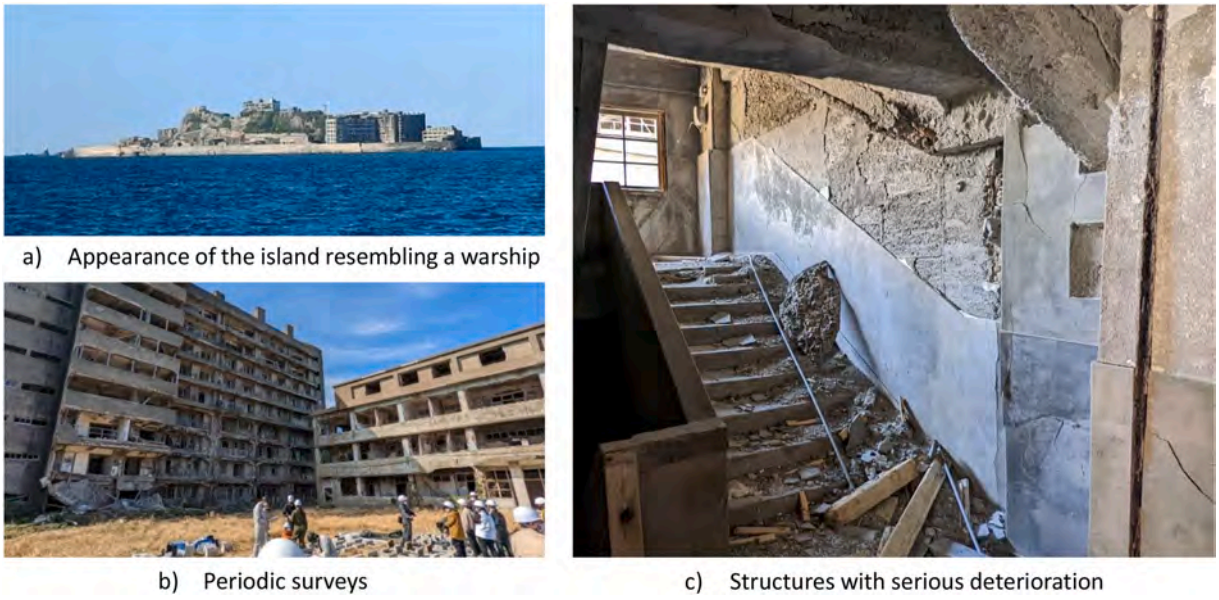

Fig. 12. Gunkanjima island.

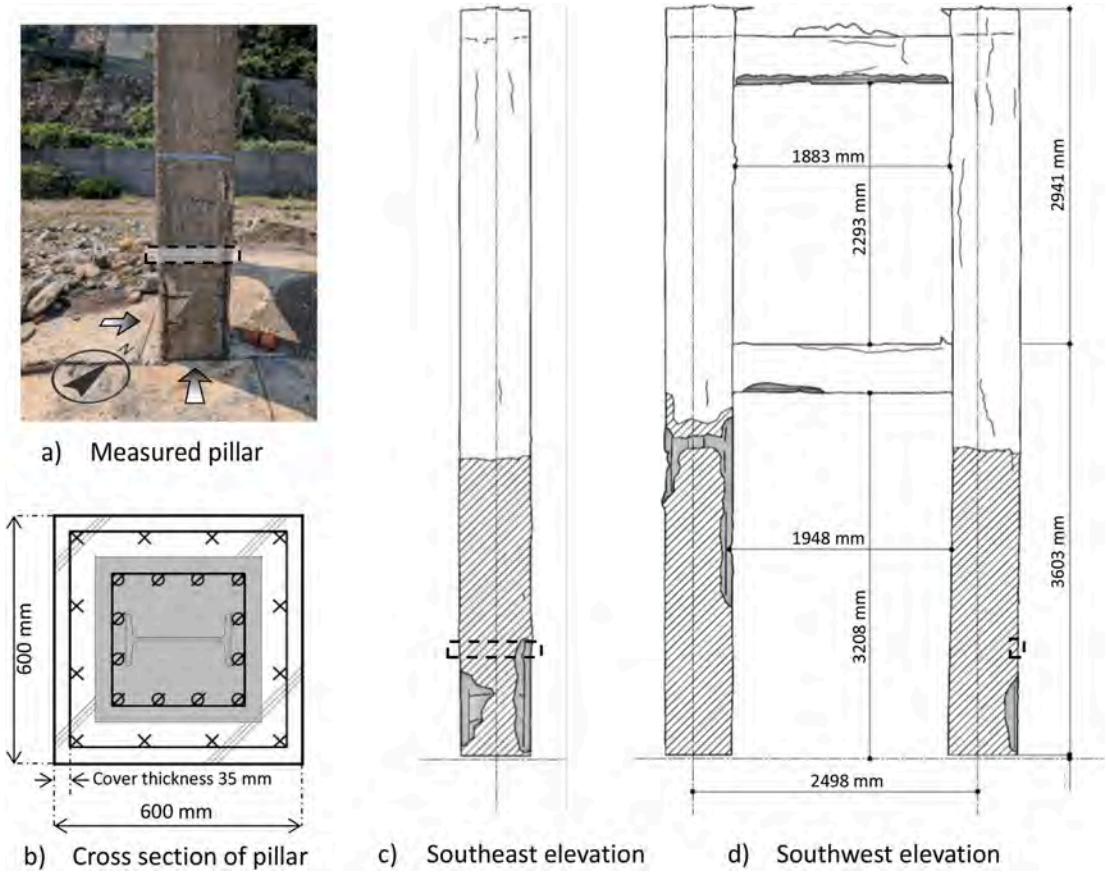

Fig. 13. Details of measured pillar.

the location of the main rebar with a cover thickness of approximately 35 mm, as identified by GPR. The strongest response was observed at the right end of the rebar where the cover was detached. We confirmed that the compactness and lightness of the camera measurement system made it possible to carry the system to the measurement site, which was not possible in the past. Because of the limited time for landing, we could not collect detailed data on the complex and characteristic deterioration of Gunkanjima island this time. Further measurements on the actual structure will be continued to obtain more data on complicated deterioration and to improve the measurement devices.

7. Conclusion

In this study, we conducted measurements using a sub-THz camera to

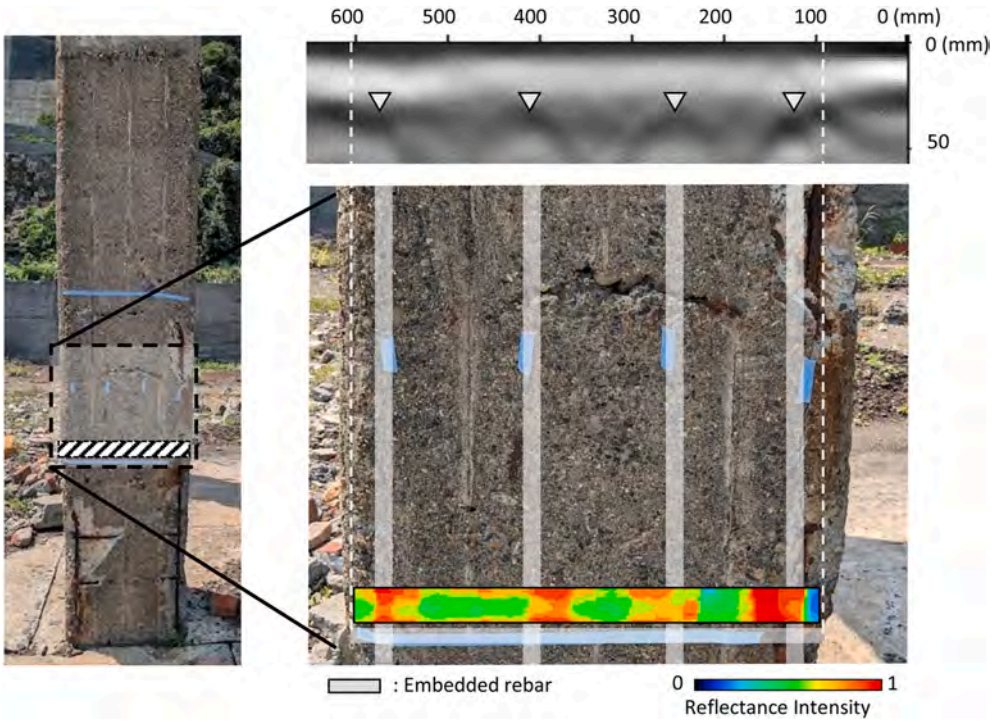

Fig. 14. Results of sub-THz wave measurements.

simulate embedded rebar and defects on the surface and inside concrete, assuming that a non-destructive inspection method using sub-THz waves will be applied to reinforced concrete structures. We then conducted actual measurements on real structures. The findings are as follows:

1) An aluminum tape placed on the back of the specimen to simulate the embedded rebar was detected up to 20 mm thickness of the specimen.
2) Field measurements at 10 GHz indicated the possibility of exploring rebars with a cover thickness of approximately 30 mm.
3) In the measurement of specimens with slits simulating cracks, detection was possible for slit widths greater than 1 mm.
4) Even when the slit was hidden by placing a 5-mm-thick mortar, detecting a slit up to 2.5 mm was possible.
5) The reflectance and transmittance varied sensitively with frequency. This fact indicates the potential for more detailed measurement with the selected appropriate frequencies. Further studies are needed to establish their relationship.
6) Camera-based measurement enables areal measurement and real-time monitoring.
7) Downsizing and weight reduction of the measurement system improved its transportability, confirming the possibility of measuring real structures.

Further applications are expected by using a camera with even higher sensitivity and multiple built-in elements and by increasing the intensity of the oscillation. In addition, THz waves are expected to be utilized as a non-destructive inspection technology for structures by combining them with THz-wave corrosion detection and ground penetrating radar (GPR), as described earlier.

CRediT authorship contribution statement

Chihiro Kobayashi: Data curation, Formal analysis, Investigation, Methodology, Visualization, Writing – original draft. **Tomoya Nishiwaki:** Conceptualization, Funding acquisition, Supervision, Writing – original draft, Writing – review & editing, Project administration. **Tadao Tanabe:** Methodology, Supervision, Writing – review & editing. **Takahiro Oohashi:** Writing – review & editing. **Hitoshi Hamasaki:** Supervision, Validation, Writing – review & editing. **Shuya Hikishima:** Investigation. **Akio Tanaka:** Investigation, Validation. **Koji Arita:** Investigation. **Sho Fujii:** Validation, Writing – review & editing. **Daisuke Sato:** Investigation, Validation. **Takeshi Kidokoro:** Investigation, Software.

Declaration of competing interest

The authors declare that they have no known competing financial interests or personal relationships that could have appeared to influence the work reported in this paper.

Data availability

Data will be made available on request.

Acknowledgement

This work was supported by JAEA Nuclear Energy S&T and Human Resource Development Project Grant Number JPJA21P21458909. We express our deep gratitude to Nagasaki City for their invaluable assistance in conducting measurements and using data from Gunkanjima. We acknowledge their support of this study.

References

Alexander, M., Beushausen, H., 2019. Durability, service life prediction, and modelling for reinforced concrete structures – review and critique. Cement Concr. Res. 122, 17–29. https://doi.org/10.1016/J.CEMCONRES.2019.04.018.

Chang, C.W., Lin, C.H., Lien, H.S., 2009. Measurement radius of reinforcing steel bar in concrete using digital image GPR. Constr Build Mater 23, 1057–1063. https://doi.org/10.1016/J.CONBUILDMAT.2008.05.018.

Cheng, C.C., Cheng, T.M., Chiang, C.H., 2008. Defect detection of concrete structures using both infrared thermography and elastic waves. Autom. ConStruct. 18, 87–92. https://doi.org/10.1016/J.AUTCON.2008.05.004.

Choi, P., Kim, D.H., Lee, B.H., Won, M.C., 2016. Application of ultrasonic shear-wave tomography to identify horizontal crack or delamination in concrete pavement and

bridge. Constr Build Mater 121, 81–91. https://doi.org/10.1016/J.CONBUILDMAT.2016.05.126.
Dash, J., Ray, S., Nallappan, K., Sasmal, S., Pesala, B., 2013. Non-destructive inspection of internal defects in concrete using continuous wave 2D terahertz imaging system. International Conference on Infrared, Millimeter, and Terahertz Waves, IRMMW-THz. https://doi.org/10.1109/IRMMW-THZ.2013.6665690.
Dinh, K., Gucunski, N., Tran, K., Novo, A., Nguyen, T., 2021. Full-resolution 3D imaging for concrete structures with dual-polarization GPR. Autom. ConStruct. 125, 103652 https://doi.org/10.1016/J.AUTCON.2021.103652.
Fan, S., Li, T., Zhou, J., Liu, X., Liu, X., Qi, H., Mu, Z., 2017. Terahertz non-destructive imaging of cracks and cracking in structures of cement-based materials. AIP Adv. 7, 115202 https://doi.org/10.1063/1.4996053/22389.
Ham, S., Popovics, J.S., 2015. Application of micro-Electro-Mechanical sensors Contactless NDT of concrete structures. Sensors 15, 9078–9096. https://doi.org/10.3390/S150409078, 15 (2015) 9078–9096.
Hara, S., Shimizu, K., Nishiwaki, T., Tanabe, T., Hmasaki, H., 2022. Evaluation of self-healing properties of Fiber-reinforced cementitious composites using reflected terahertz waves. Proceeding of International Conference on Regeneration and Conservation of Structures.
Hugenschmidt, J., Mastrangelo, R., 2006. GPR inspection of concrete bridges. Cem. Concr. Compos. 28, 384–392. https://doi.org/10.1016/J.CEMCONCOMP.2006.02.016.
Im, K.H., Kim, S.K., Hsu, D.K., Jung, J.A., 2017. Coating thickness characterization of composite materials using terahertz waves. Mater. Sci. Forum 878, 70–73. https://doi.org/10.4028/WWW.SCIENTIFIC.NET/MSF.878.70.
Inuzuka, M., Kouzuma, Y., Sugioka, N., Fukunaga, K., Tateishi, T., 2017. Investigation of layer structure of the takamatsuzuka mural paintings by terahertz imaging technique. J. Infrared, Millim. Terahertz Waves 38, 380–389. https://doi.org/10.1007/S10762-017-0365-2/FIGURES/9.
Janků, M., Březina, I., Grošek, J., 2017. Use of infrared thermography to detect defects on concrete bridges. Procedia Eng. 190, 62–69. https://doi.org/10.1016/J.PROENG.2017.05.308.
Kariya, H., Sato, A., Tanabe, T., Saito, K., Nishihara, K., Taniyama, A., Oyama, Y., 2013. Non-destructive evaluation of a corroded metal surface using terahertz wave. ECS Trans. 50, 81–88. https://doi.org/10.1149/05050.0081ECST/XML.
Kazemi, M., Madandoust, R., de Brito, J., 2019. Compressive strength assessment of recycled aggregate concrete using Schmidt rebound hammer and core testing. Constr Build Mater 224, 630–638. https://doi.org/10.1016/J.CONBUILDMAT.2019.07.110.
Kobayashi, C., Nishiwaki, T., Hara, S., Tanabe, T., Oohashi, T., Hamasaki, H., Hikishima, S., Tanaka, A., Arita, K., 2023. Fundamental research on non-destructive testing of reinforced concrete structures using sub-terahertz reflected waves. MATEC Web of Conferences 378, 04007. https://doi.org/10.1051/MATECCONF/202337804007.
Kotyaev, O., Shimada, Y., Hashimoto, K., 2006. Laser-based non-destructive detection of inner flaws in concrete with the use of lamb waves. 9th European Conference on NDT - September 2006 - Berlin (Germany). https://www.ndt.net/?id=3601.
Krimi, S., Klier, J., Jonuscheit, J., Von Freymann, G., Urbansky, R., Beigang, R., 2016. Highly accurate thickness measurement of multi-layered automotive paints using terahertz technology. Appl. Phys. Lett. 109 https://doi.org/10.1063/1.4955407/32936.
Krügener, K., Ornik, J., Schneider, L.M., Jäckel, A., Koch-Dandolo, C.L., Castro-Camus, E., Riedl-Siedow, N., Koch, M., Viöl, W., 2020. Terahertz inspection of buildings and architectural art. Appl. Sci. 10 https://doi.org/10.3390/APP10155166.
Kurahashi, S., Mikami, K., Kitamura, T., Hasegawa, N., Okada, H., Kondo, S., Nishikino, M., Kawachi, T., Shimada, Y., 2018. Demonstration of 25-Hz-inspection-speed laser remote sensing for internal concrete defects. https://doi.org/10.1117/1.JRS.12.015009.
Lambert, F.E.M., Reyes-Reyes, E.S., Hernandez-Cardoso, G.G., Gomez-Sepulveda, A.M., Castro-Camus, E., 2020. In situ determination of the state of conservation of paint coatings on the kiosk of guadalajara using terahertz time-domain spectroscopy. J. Infrared, Millim. Terahertz Waves 41, 355–364. https://doi.org/10.1007/S10762-019-00645-6/FIGURES/7.
Laurens, S., Balayssac, J.P., Rhazi, J., Klysz, G., Arliguie, G., 2005. Non-destructive evaluation of concrete moisture by GPR: experimental study and direct modeling. Mater. Struct. 38 (9 38), 827–832. https://doi.org/10.1007/BF02481655, 2005.
Lawson, I., Lawson, I., Danso, K.A., Odoi, H.C., Adjei, C.A., Quashie, F.K., Mumuni, I.I., Ibrahim, I.S., 2011. Non-destructive evaluation of concrete using ultrasonic pulse velocity. Article in Research Journal of Applied Sciences, Engineering and Technology 3, 499–504. https://www.researchgate.net/publication/265144573.
Liu, H., Lin, C., Cui, J., Fan, L., Xie, X., Spencer, B.F., 2020. Detection and localization of rebar in concrete by deep learning using ground penetrating radar. Autom. ConStruct. 118, 103279 https://doi.org/10.1016/J.AUTCON.2020.103279.
Michel, A., Pease, B.J., Geiker, M.R., Stang, H., Olesen, J.F., 2011. Monitoring reinforcement corrosion and corrosion-induced cracking using non-destructive x-ray attenuation measurements. Cement Concr. Res. 41, 1085–1094. https://doi.org/10.1016/J.CEMCONRES.2011.06.006.
Mori, K., Spagnoli, A., Murakami, Y., Kondo, G., Torigoe, I., 2002. A new non-contacting non-destructive testing method for defect detection in concrete. NDT E Int. 35, 399–406. https://doi.org/10.1016/S0963-8695(02)00009-9.
Nakamura, Y., Kariya, H., Sato, A., Tanabe, T., Nishihara, K., Taniyama, A., Nakajima, K., Maeda, K., Oyama, Y., 2014. Nondestructive corrosion diagnosis of painted hot-dip galvanizing steel sheets by using THz spectral imaging. Corrosion Eng. 63, 411–416. https://doi.org/10.3103/S0892422814090043.
Neu, J., Schmuttenmaer, C.A., 2018. Tutorial: an introduction to terahertz time domain spectroscopy (THz-TDS). J. Appl. Phys. 124, 231101 https://doi.org/10.1063/1.5047659/13481510/231101_1_ACCEPTED_MANUSCRIPT.PDF.
Nishiwaki, T., Shimizu, K., Tanabe, T., Gardner, D., Maddalena, R., 2023. Terahertz (THz) wave imaging in civil engineering to assess self-healing of fiber-reinforced cementitious composites (FRCC). J. Adv. Concr. Technol. 21, 58–75. https://doi.org/10.3151/JACT.21.58.
Omar, T., Nehdi, M.L., 2017. Remote sensing of concrete bridge decks using unmanned aerial vehicle infrared thermography. Autom. ConStruct. 83, 360–371. https://doi.org/10.1016/J.AUTCON.2017.06.024.
Oyama, Y., Zhen, L., Tanabe, T., Kagaya, M., 2009. Sub-terahertz imaging of defects in building blocks. NDT E Int. 42, 28–33. https://doi.org/10.1016/J.NDTEINT.2008.08.002.
Oyama, Y., Yamagata, T., Kariya, H., Tanabe, T., Saito, K., 2013. Non-destructive inspection of copper corrosion via coherent terahertz light source. ECS Trans. 50, 89–98. https://doi.org/10.1149/05050.0089ECST/XML.
Piesiewicz, R., Jansen, C., Wietzke, S., Mittleman, D., Koch, M., Kürner, T., 2007. Properties of building and plastic materials in the THz range. Int. J. Infrared Millimet. Waves 28, 363–371. https://doi.org/10.1007/s10762-007-9217-9.
Shimada, Y., Kotyaev, O., Kurahashi, S., Yasuda, N., Misaki, N., Takayama, Y., Soga, T., 2019. Development of laser-based remote sensing technique for detecting defects of concrete lining. Electron. Commun. Jpn. 102, 12–18. https://doi.org/10.1002/ECJ.12168.
Skarzyński, J. Tejchman, 2016. Experimental investigations of fracture process in concrete by means of X-ray micro-computed tomography. Strain 52, 26–45. https://doi.org/10.1111/STR.12168.
Sonoda, Y., Lu, C., Yin, Y., 2023. Basic research on usefulness of convolutional autoencoders in detecting defects in concrete using hammering sound. Struct. Health Monit. 22, 2231–2250. https://doi.org/10.1177/14759217221122296/ASSET/IMAGES/LARGE/10.1177_14759217221122296-FIG20.JPEG.
Su, K., Shen, Y.C., Zeitler, J.A., 2014. Terahertz sensor for non-contact thickness and quality measurement of automobile paints of varying complexity. IEEE Trans Terahertz Sci Technol 4, 432–439. https://doi.org/10.1109/TTHZ.2014.2325393.
Sugimoto, K., Sugimoto, T., Utagawa, N., Katakura, K., 2016. The non-contact acoustic inspection method for concrete structures using the defect detection algorithm that combined spectrum entropy with vibrational energy ratio. http://creativecommons.org/licenses/by/3.0/. (Accessed 21 October 2023).
Takahashi, S., Hamano, T., Nakajima, K., Tanabe, T., Oyama, Y., 2014. Observation of damage in insulated copper cables by THz imaging. NDT E Int. 61, 75–79. https://doi.org/10.1016/J.NDTEINT.2013.10.004.
Tanabe, T., Oyama, Y., 2019. THz non-destructive visualization of disconnection and corrosion status covered with opaque insulator. IEEJ Transactions on Electronics, Information and Systems 139, 149–153. https://doi.org/10.1541/ieejeiss.139.149.
Tanabe, T., Watanabe, K., Oyama, Y., Seo, K., 2010. Polarization sensitive THz absorption spectroscopy for the evaluation of uniaxially deformed ultra-high molecular weight polyethylene. NDT E Int. 43, 329–333. https://doi.org/10.1016/J.NDTEINT.2010.03.001.
Tanabe, T., Kanai, T., Kuroo, K., Nishiwaki, T., Oyama, Y., 2018. Non-contact terahertz inspection of water content in concrete of infrastructure buildings. World J. Eng. Technol. 6, 275–281. https://doi.org/10.4236/wjet.2018.62016.
Tarussov, A., Vandry, M., De La Haza, A., 2013. Condition assessment of concrete structures using a new analysis method: ground-penetrating radar computer-assisted visual interpretation. Constr Build Mater 38, 1246–1254. https://doi.org/10.1016/J.CONBUILDMAT.2012.05.026.
Togo, H., Kojima, T., Mochizuki, S., Kukutsu, N., 2012. Millimeter-wave imaging for detecting surface cracks on concrete Pole covered with bill-posting prevention sheet. NTT Tech. Rev. 10. https://www.ntt-review.jp/archive/ntttechnical.php?contents=ntr201202fa2.html. (Accessed 21 October 2023).
Tokizane, Y., Yamaguchi, T., Minamikawa, T., Hase, E., Yamaguchi, K., Suzuki, A., Ueda, T., Yasui, T., 2022. Ultralow-frequency ultranarrow-bandwidth coherent terahertz imaging for nondestructive testing of mortar material. Opt Express 30 (3), 4392–4401 30. https://doi.org/10.1364/OE.449092, 4392–4401.
Tripathi, S.R., Ogura, H., kawagoe, H., Inoue, H., Hasegawa, T., Takeya, K., Kawase, K., 2012. Measurement of chloride ion concentration in concrete structures using terahertz time domain spectroscopy (THz-TDS). Corrosion Sci. 62, 5–10. https://doi.org/10.1016/J.CORSCI.2012.05.005.
Wiwatrojanagul, P., Sahamitmongkol, R., Tangtermsirikul, S., Khamsemanan, N., 2017. A new method to determine locations of rebars and estimate cover thickness of RC structures using GPR data. Constr Build Mater 140, 257–273. https://doi.org/10.1016/J.CONBUILDMAT.2017.02.126.
Xu, Y., Jiang, X., 2022. Nondestructive testing and imaging of corrosion thickness of steel plates using THz-TDS. Infrared Phys. Technol. 127, 104467 https://doi.org/10.1016/J.INFRARED.2022.104467.
Zhang, G., Harichandran, R.S., Ramuhalli, P., 2012. An automatic impact-based delamination detection system for concrete bridge decks. NDT E Int. 45, 120–127. https://doi.org/10.1016/J.NDTEINT.2011.09.013.